Electronic Supplementary Material (ESI) for Physical Chemistry Chemical Physics.

Supporting information: Predicting ^{17}O NMR chemical shifts of polyoxometalates using density functional theory.

Rupali Sharma[1], Jie Zhang[1], and C. André Ohlin[1]

[1]School of Chemistry, Monash University, Victoria, Australia

School of Chemistry, Monash University, Victoria 3800 Australia

Contents

List of Tables

S1 Abbreviations used in the Supporting Information. 5
S2 Maximum absolute error and average absolute error in predicted vs crystal structure bond distances of Nb_{10} and Ti_2Nb_8 for different exchange correlation functionals. Geometries were optimised using the indicated XC functionals and lanl2dz (Ti, Nb) and cc-pvtz (O). 5
S3 Absolute maximum (AME) and average errors (AAE) in predicted shifts vs observed shifts for Nb_{10} after linear regression has been applied. Slope and intercept for the regression that has been applied is also indicated. OPBE(25) indicates OPBE with 0.75 PBE exchange and 0.25 HF exchange. 7
S4 ^{17}O NMR shifts in ppm relative to water of $[Nb_{10}O_{28}]^{6-}$ computed with different amounts of exact HF exchange used with the PBE exchange/correlation functional, where XC=n·HF_X+(1-n)·PBE_x + PBE_c. PBE_x is the exchange functional of the PBE XC and PBE_c is the correlation one. All computations used the structure optimised at PBE0/cc-pvtz(H-Ar), lanl2dz (K-) and were performed with def2-tzvp. 8
S5 Experimentally determined ^{17}O NMR shifts of polyoxovanadates. The lettering indicates different oxygen sites, the type of which are specified in parentheses. See original publication for assignment. Data used in regression is indicated with *. 11
S6 Computed non-regressed ^{17}O NMR shifts of polyoxovanadates at PBE0/def2-tzvp//PBE0/cc-pvtz(H-Ar), lanl2dz(K-). 11
S7 Experimentally determined ^{17}O NMR shifts of polyoxoniobates. The lettering indicates different oxygen sites, the type of which are specified in parentheses. See original publication and figures S10-S11 for assignment. Data used in regression is indicated with *. 12
S8 Computed non-regressed ^{17}O NMR shifts of polyoxoniobates at PBE0/def2-tzvp//PBE0/cc-pvtz(H-Ar), lanl2dz(K-). 13
S9 Experimentally determined ^{17}O NMR shifts of polyoxotantalates. The lettering indicates different oxygen sites, the type of which are specified in parentheses. See original publication and figures S10-S11 for assignment. Data used in regression is indicated with *. 14
S10 Computed non-regressed ^{17}O NMR shifts of polyoxotantalates at PBE0/def2-tzvp//PBE0/cc-pvtz(H-Ar), lanl2dz(K-). 14
S11 Experimentally determined ^{17}O NMR shifts of polyoxomolybdates. The lettering indicates different oxygen sites, the type of which are specified in parentheses. See original publication and figures S10-S11 for assignment. Data used in regression is indicated with *. 15
S12 Computed non-regressed ^{17}O NMR shifts of polyoxomolybdates at PBE0/def2-tzvp//PBE0/cc-pvtz(H-Ar), lanl2dz(K-). 16
S13 Experimentally determined ^{17}O NMR shifts of polyoxotungstates. The lettering indicates different oxygen sites, the type of which are specified in parentheses. See original publication and figures S10-S11 for assignment. Data used in regression is indicated with *. 17
S14 Computed non-regressed ^{17}O NMR shifts of polyoxotungstates at PBE0/def2-tzvp//PBE0/cc-pvtz(H-Ar), lanl2dz(K-). 18
S15 Computed non-regressed ^{17}O NMR shifts in ppm of protonated and unprotonated structures of $[Nb_6O_{19}]^{8-}$ at PBE0/def2-tzvp//PBE0/cc-pvtz(H-Ar), lanl2dz(K-). The different isomers are listed in the same order as in figure S8. The lowest energy isomers at pbe0/def2-tzvp are marked with bold; $\Delta\epsilon$ is given relative to the lowest energy isomer for each protonation state. 20
S16 Extracted chemical shifts for the η-oxygen site in the hexaniobate ion as a function of pH. The data was extracted from figure 4 in Black *et al.*, *J. Am. Chem. Soc.*, **2006**, *128*, 14712-14720. 21
S17 Extracted chemical shifts for the μ_2-oxygen site in the hexaniobate ion as a function of pH. The data was extracted from figure 4 in Black *et al.*, *J. Am. Chem. Soc.*, **2006**, *128*, 14712-14720. 24

S18 Extracted chemical shifts for the μ_6-oxygen site in the hexaniobate ion as a function of pH. The data was extracted from figure 4 in Black *et al.*, *J. Am. Chem. Soc.*, **2006**, *128*, 14712-14720. 25

List of Figures

S1 a) Maximum (red) and average (blue) absolute errors in calculated bond distances relative to the crystal structure for $[Nb_{10}O_{28}]^{6-}$ for different basis sets. b) Error in calculated, non-regressed shift vs observed shift for structures of $[Nb_{10}O_{28}]^{6-}$ optimised using PBE0 and cc-pvdz(H-AR),lanl2dz (K-, blue circles), cc-pvtz (H-Ar), lanl2dz (K-) (blue squares), def2-svp (red circles) and def2-tzvp (red squares). The NMR shifts were all calculated using PBE0/def2-tzvp with PCM (water). The maximum and absolute errors for the linearly regressed vs observed shifts are 7.45 and 4.01 (cc-pvdz/lanl2dz), 6.61 and 3.10 (cc-pvtz/lanl2dz), 7.45 and 4.02 (def2-svp), and 8.62 and 4.18 (def2-tzvp) ppm, respectively 6

S2 Effect of the basis set in the NMR shift calculation on the calculated non-regressed ^{17}O NMR chemical shift of $[Nb_{10}O_{28}]^{6-}$ (a), $[TiNb_9O_{28}]^{7-}$ (b) and $[Ti_2Nb_8O_{28}]^{8-}$ (c). cc-pvtz/lanl2dz indicates that cc-pvtz was used for H-Ar and lanl2dz for all elements from K and above. All shift calculations were done using PBE0 and with implicit solvation using PCM (water), and using a structure optimised using PBE0, and cc-pvtz (H-Ar) and lanl2dz (K-). 7

S3 Maximum (red) and average (blue) absolute errors in calculated, linearly regressed ^{17}O NMR shifts using the crystal structures of $[Nb_{10}O_{28}]^{6-}$ (a), $[TiNb_9O_{28}]^{7-}$ (b) and $[Ti_2Nb_8O_{28}]^{8-}$ (c). Note that the large errors for $[TiNb_9O_{28}]^{7-}$ is due to the crystal structure being symmetric because of averaging of bond parameters from each central metal sites having 50% Ti/50% Nb occupancy. Note that the shifts were computed using cc-pvtz(H-Ar), lanl2dz(K-) and not def2-tzvp. 8

S4 Computation of the ^{17}O NMR chemical shift of $[Nb_{10}O_{28}]^{6-}$ as a function of exchange correlation functional used to optimise the structure in conjunction with cc-pvtz (H-Ar) and lanl2dz (K-). All NMR shifts were were calculated using PBE0/def2-tzvp. a) Error in computed shift as a function of observed shift. Non-hybrid DFT functionals in black, hybrid DFT functionals in red and long-range corrected functionals in blue. b) Maximum and average error in computed shift as a function of exchange correlation functional. 9

S5 a) Effect on the maximum and average error in the calculated linearly regressed ^{17}O NMR chemical shift of $[Nb_{10}O_{28}]^{6-}$ of varying the HF-exchange-to-PBE-exchange ratio using n in the exchange correlation functional XC=n·HF_{ex}+(n-1)·PBE_{ex})+PBE_{corr} . For the pure PBE GGA n=0.0. For the hybrid functional PBE0 n=0.25. All shift calculations were done using def2-tzvp and implicit solvation using PCM (water) with the structure optimised at PBE0/ccpvtz(H-Ar), lanl2dz (K-). 10

S6 Effect on the calculated non-regressed ^{17}O NMR chemical shift of $[Nb_{10}O_{28}]^{6-}$ of varying the HF-exchange-to-PW91-exchange ratio using n in the exchange correlation functional XC=n·HF_{ex}+(n-1)·$PW91_{ex}$)+$PW91_{corr}$, and b) effect on the maximum and average error in the calculated linearly regressed ^{17}O NMR chemical shift. All shift calculations were done using def2-tzvp and with implicit solvation using PCM (water), and using a structure optimised at PBE0/cc-pvtz(H-Ar), lanl2dz(K-). 19

S7 Predicted vs observed ^{17}O NMR chemical shifts for all the compounds in the test set. The coefficient of determination is 0.993. 21

S8 The lowest energy isomers for each protonation state are framed. From left to right, top row (energy in parenthesis): $[HNb_6O_{19}]^{7-}$ (-1773.32865682 a.u.), $[H_2Nb_6O_{19}]^{6-}$ (-1773.84487818 a.u.), $[H_2Nb_6O_{19}]^{6-}$ (-1773.84142771 a.u.) and $[H_2Nb_6O_{19}]^{6-}$ (-1773.8376808 a.u.). Second row: $[H_2Nb_6O_{19}]^{6-}$ (-1773.83737179 a.u.), $[H_2Nb_6O_{19}]^{6-}$ (-1773.84557801 a.u.), $[H_2Nb_6O_{19}]^{6-}$ (-1773.84547981 a.u.) and $[H_2Nb_6O_{19}]^{6-}$ (-1773.8406571 a.u.). Third row: $[H_2Nb_6O_{19}]^{6-}$ (-1773.84094689 a.u.), $[H_3Nb_6O_{19}]^{6-}$ (-1774.3391972 a.u.), $[H_3Nb_6O_{19}]^{6-}$ (-1774.338802 a.u.) and $[H_3Nb_6O_{19}]^{6-}$ (-1774.3476813 a.u.). Fourth row: $[H_3Nb_6O_{19}]^{6-}$ (-1774.33818085 a.u.), $[H_3Nb_6O_{19}]^{6-}$ (-1774.34387887 a.u.), $[H_3Nb_6O_{19}]^{6-}$ (-1774.34226680 a.u.) and $[H_3Nb_6O_{19}]^{6-}$ (-1774.32708771 a.u.). Fifth row: $[H_3Nb_6O_{19}]^{6-}$ (-1774.32677228 a.u.), $[H_3Nb_6O_{19}]^{6-}$ (-1774.34242317 a.u.), $[H_3Nb_6O_{19}]^{6-}$ (-1774.32713339 a.u.) and $[H_3Nb_6O_{19}]^{6-}$ (-1774.34196575 a.u.). Sixth row: $[H_3Nb_6O_{19}]^{6-}$ (-1774.32712675 a.u.), $[H_3Nb_6O_{19}]^{6-}$ (-1774.33816727 a.u.), $[H_3Nb_6O_{19}]^{6-}$ (-1774.33525822 a.u.) and $[H_3Nb_6O_{19}]^{6-}$ (-1774.32831278 a.u.). Seventh row: $[H_3Nb_6O_{19}]^{6-}$ (-1774.33525822 a.u.), $[H_3Nb_6O_{19}]^{6-}$ (-1774.34200367 a.u.), $[H_3Nb_6O_{19}]^{6-}$ (-1774.31576440 a.u.) and $[H_3Nb_6O_{19}]^{6-}$ (-1774.32712033 a.u.). Eighth row: $[H_3Nb_6O_{19}]^{6-}$ (-1774.34242370 a.u.), $[H_3Nb_6O_{19}]^{6-}$ (-1774.32708035 a.u.) and $[H_3Nb_6O_{19}]^{6-}$ (-1774.32677621 a.u.) 23
S9 Speciation of the hexaniobate Lindqvist ion as a function of pH simulated using the Octave code in listings S1 and S2. 24
S10 Key I to oxygen types referred to in tables S5-S14. Row 1, left: $[V_2O_7]^{4-}$. Right: $[V_4O_{12}]^{4-}$. Row 2, left: $[M_{10}O_{28}]^{x-}$. Right: $[V_9MoO_{28}]^{5-}$. Row 3, left: cis–$[V_8Mo_2O_{28}]^{4-}$. Right: trans–$[V_8Mo_2O_{28}]^{4-}$. Row 4, left: $[M_6O_{19}]^{x-}$. Right: $[TiNb_9O_{28}]^{7-}$. 26
S11 Key II to oxygen types referred to in tables S5-S14. Row 1, left: $[M,M_5O_{19}]^{x-}$ and $[M,(OMe)M_5O_{18}]^{x-}$. Right: $[M,_2M_4O_{19}]^{x-}$. Row 2, left: $H_n[M,Mo_6O_{24}]^{x-}$. Right: $[M_7O_{24}]^{6-}$. Row 3, left: α–$[Mo_8O_{26}]^{4-}$. Right: β–$[Mo_8O_{26}]^{4-}$. Row 4, left: $[M,M_{12}OO_{40}]^{x-}$. Right: $[W_{10}O_{32}]^{4-}$. 27

Listings

S1 control.m 19
S2 speciation.m 19

Table S1: Abbreviations used in the Supporting Information.

Abbreviation	Explanation
ACN	Acetonitrile
Aq.	Water
DCM	Dichloromethane
Nb_{10}	$[Nb_{10}O_{28}]^{6-}$
TBA	Tetrabutylammonium
$TiNb_9$	$[Ti_2Nb_8O_{28}]^{7-}$
Ti_2Nb_8	$[Ti_2Nb_8O_{28}]^{8-}$
TMA	Tetramethylammonium

Table S2: Maximum absolute error and average absolute error in predicted vs crystal structure bond distances of Nb_{10} and Ti_2Nb_8 for different exchange correlation functionals. Geometries were optimised using the indicated XC functionals and lanl2dz (Ti, Nb) and cc-pvtz (O).

Molecule	Functional	Maximum absolute error (pm)	Average Absolute Error (pm)
Nb_{10}	BP86	5.51	3.18
	PW91	5.10	2.93
	PBE	5.21	2.42
	M06L	3.66	1.72
	B3LYP	5.21	2.42
	PBE0	2.52	1.01
	M06	5.11	2.76
	CAM-B3LYP	3.35	1.15
	lc-ωPBE	2.83	0.99
	ωB97XD	3.70	1.39
Ti_2Nb_8	BP86	9.05	3.73
	PW91	8.67	3.46
	PBE	8.92	3.60
	M06L	9.22	3.27
	B3LYP	8.73	2.97
	PBE0	6.15	1.72
	M06	7.33	2.30
	CAM-B3LYP	6.54	1.75
	lc-ωPBE	4.25	1.32
	ωB97XD	7.22	2.01

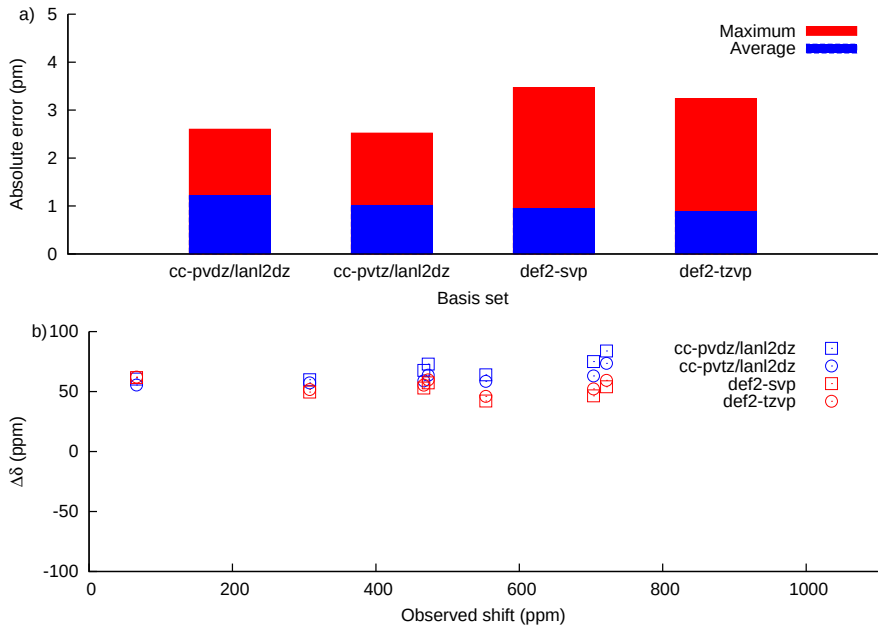

Figure S1: a) Maximum (red) and average (blue) absolute errors in calculated bond distances relative to the crystal structure for $[Nb_{10}O_{28}]^{6-}$ for different basis sets. b) Error in calculated, non-regressed shift vs observed shift for structures of $[Nb_{10}O_{28}]^{6-}$ optimised using PBE0 and cc-pvdz(H-AR),lanl2dz (K-, blue circles), cc-pvtz (H-Ar), lanl2dz (K-) (blue squares), def2-svp (red circles) and def2-tzvp (red squares). The NMR shifts were all calculated using PBE0/def2-tzvp with PCM (water). The maximum and absolute errors for the linearly regressed vs observed shifts are 7.45 and 4.01 (cc-pvdz/lanl2dz), 6.61 and 3.10 (cc-pvtz/lanl2dz), 7.45 and 4.02 (def2-svp), and 8.62 and 4.18 (def2-tzvp) ppm, respectively

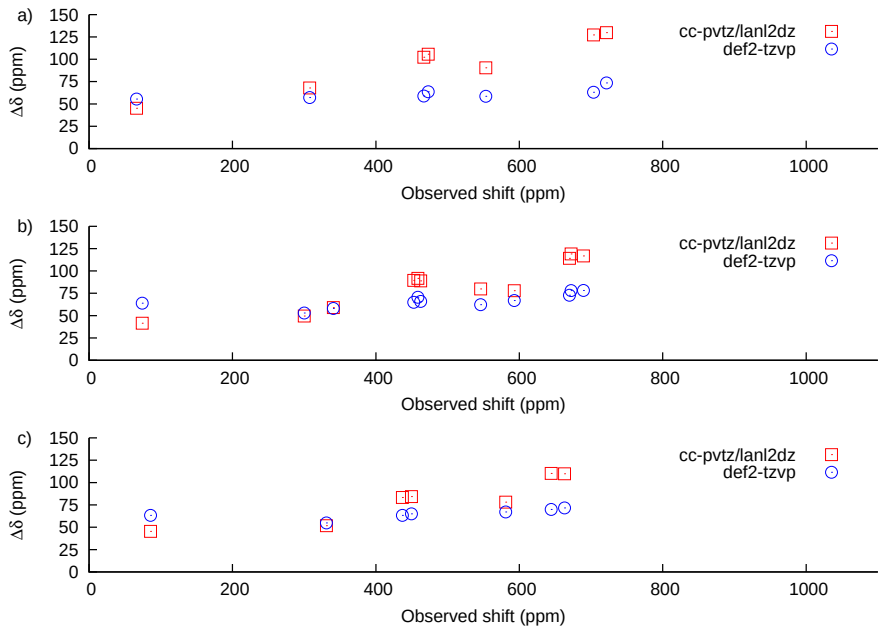

Figure S2: Effect of the basis set in the NMR shift calculation on the calculated non-regressed ^{17}O NMR chemical shift of $[Nb_{10}O_{28}]^{6-}$ (a), $[TiNb_9O_{28}]^{7-}$ (b) and $[Ti_2Nb_8O_{28}]^{8-}$ (c). cc-pvtz/lanl2dz indicates that cc-pvtz was used for H-Ar and lanl2dz for all elements from K and above. All shift calculations were done using PBE0 and with implicit solvation using PCM (water), and using a structure optimised using PBE0, and cc-pvtz (H-Ar) and lanl2dz (K-).

Table S3: Absolute maximum (AME) and average errors (AAE) in predicted shifts vs observed shifts for Nb_{10} after linear regression has been applied. Slope and intercept for the regression that has been applied is also indicated. OPBE(25) indicates OPBE with 0.75 PBE exchange and 0.25 HF exchange.

Entry	Functional	AME (ppm)	AAE (ppm)	Slope	Intercept (ppm)	r^2
1	BP86	20.22	11.67	1.12	-117	0.996
2	PBE	20.58	11.77	1.12	-118	0.996
3	OPBE	22.28	12.14	1.14	-115	0.996
4	PW91	20.55	11.77	1.11	-118	0.996
5	M06L	21.19	15.48	1.18	-86	0.994
6	B3LYP	7.49	3.81	0.99	-63	0.999(6)
7	PBE0	6.61	3.10	0.98	-51	0.999(7)
8	OPBE(25)	7.11	3.62	1.00	-48	0.999(6)
9	mPW91	6.43	3.04	0.97	-51	0.999(7)
10	M06	6.19	2.61	0.95	-57	0.999(8)
11	CAM-B3LYP	11.41	7.40	0.95	-23	0.999
12	lc-ωPBE	25.27	15.94	0.95	8.7	0.994
13	ωB97XD	10.45	7.29	0.95	-19	0.999

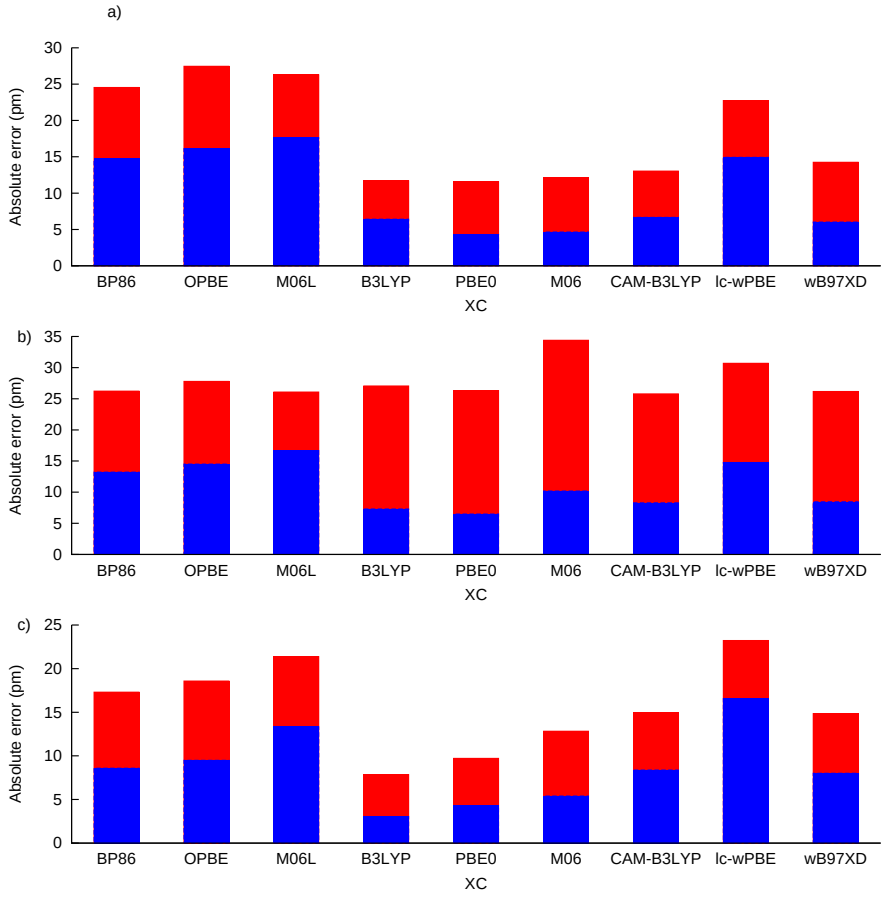

Figure S3: Maximum (red) and average (blue) absolute errors in calculated, linearly regressed ^{17}O NMR shifts using the crystal structures of $[Nb_{10}O_{28}]^{6-}$ (a), $[TiNb_9O_{28}]^{7-}$ (b) and $[Ti_2Nb_8O_{28}]^{8-}$ (c). Note that the large errors for $[TiNb_9O_{28}]^{7-}$ is due to the crystal structure being symmetric because of averaging of bond parameters from each central metal sites having 50% Ti/50% Nb occupancy. Note that the shifts were computed using cc-pvtz(H-Ar), lanl2dz(K-) and not def2-tzvp.

Table S4: ^{17}O NMR shifts in ppm relative to water of $[Nb_{10}O_{28}]^{6-}$ computed with different amounts of exact HF exchange used with the PBE exchange/correlation functional, where XC=n·HF_X+(1-n)·PBE_x + PBE_c. PBE_x is the exchange functional of the PBE XC and PBE_c is the correlation one. All computations used the structure optimised at PBE0/cc-pvtz(H-Ar), lanl2dz (K-) and were performed with def2-tzvp.

n	A (Nb_6O)	B (Nb_3−O)	C (Nb_2−O)	D (Nb_2−O)	E (Nb_2−O)	F (Nb=O)	G (Nb=O)
Experimental	66.28	307.63	466.85	472.97	553.3	703.51	721.52
0.00	151.8693	387.1852	535.9396	547.5211	601.1162	717.8359	745.5329
0.05	145.4058	383.0118	534.8875	546.2284	603.8797	727. 9502	755.6541
0.15	133.1047	374.1881	531.2756	542.2933	608.4974	747.6751	775.5414
0.20	127.2832	369.5711	528.7474	539.6810	610.3316	757.2367	785.2517
0.25	121.6874	364.8398	525.7640	536.6640	611.8384	766.5670	794.7706
0.30	116.3049	360.0098	522.3527	533.2634	613.0110	775.6402	804.0718

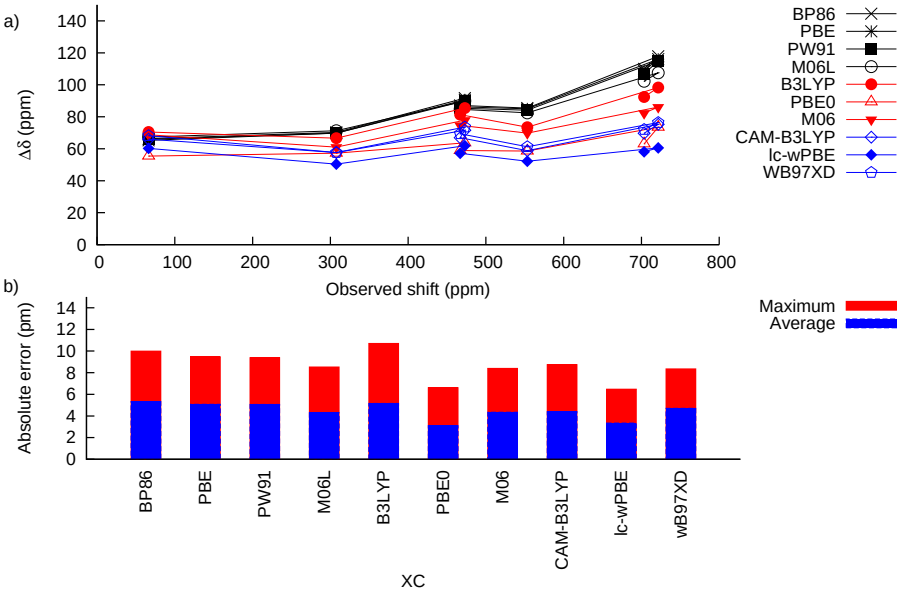

Figure S4: Computation of the ^{17}O NMR chemical shift of $[Nb_{10}O_{28}]^{6-}$ as a function of exchange correlation functional used to optimise the structure in conjunction with cc-pvtz (H-Ar) and lanl2dz (K-). All NMR shifts were were calculated using PBE0/def2-tzvp. a) Error in computed shift as a function of observed shift. Non-hybrid DFT functionals in black, hybrid DFT functionals in red and long-range corrected functionals in blue. b) Maximum and average error in computed shift as a function of exchange correlation functional.

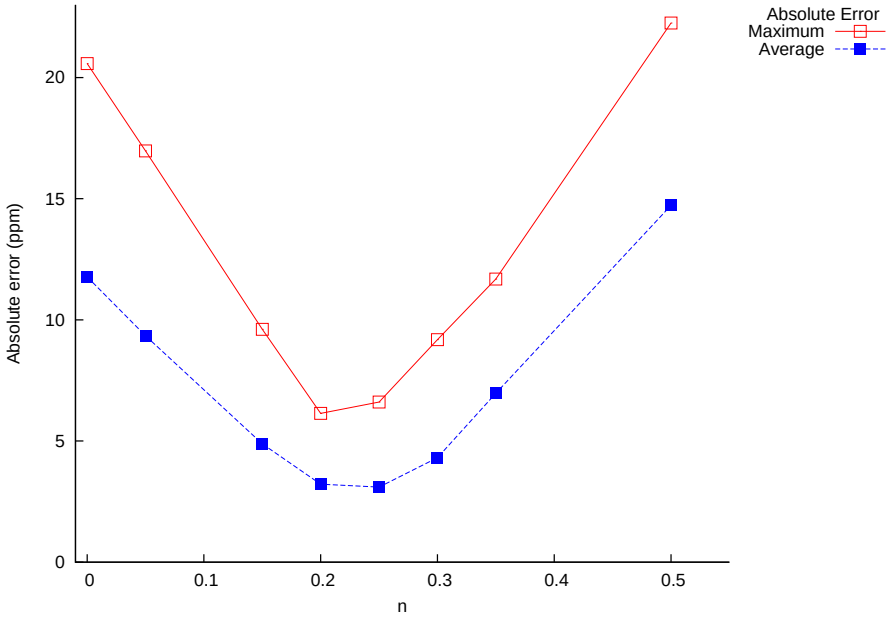

Figure S5: a) Effect on the maximum and average error in the calculated linearly regressed ^{17}O NMR chemical shift of $[Nb_{10}O_{28}]^{6-}$ of varying the HF-exchange-to-PBE-exchange ratio using n in the exchange correlation functional XC=n·HF_{ex}+(n-1)·PBE_{ex})+PBE_{corr} . For the pure PBE GGA n=0.0. For the hybrid functional PBE0 n=0.25. All shift calculations were done using def2-tzvp and implicit solvation using PCM (water) with the structure optimised at PBE0/ccpvtz(H-Ar), lanl2dz (K-).

Table S5: Experimentally determined ^{17}O NMR shifts of polyoxovanadates. The lettering indicates different oxygen sites, the type of which are specified in parentheses. See original publication for assignment. Data used in regression is indicated with *.

Entry	Anion	A μ_6-O	B μ_3-O	C μ_2-O	D μ_2-O	E μ_2-O	F η-O (V)	G η-O (V)	H OV_5M	I OV_2M	J OM_3	K VOM	L OM	Cation, Solvent [Ref.]
1*	$[V_2O_7]^{4-}$			405			696							$[Na]^+$, Aq.[b] [1]
2*	$[V_4O_{12}]^{4-}$			472			928							$[Na]^+$, Aq., pH 7 [1]
3	$[V_{10}O_{28}]^{6-}$	63	397	765	790	895	1140	1150						$[Na]^+$, Aq. pH 5.4 [2]
4		72	378	759	803	904	1160[a]							$[Na]^+$, Aq. pH 4.5 [3]
5		67	396	764	790	898	1150[a]							$[Na]^+$, Aq. pH 5.0 [3]
6		63	400	764	786	895	1146[a]							$[Na]^+$, Aq. pH 5.5 [3]
7*		62	406	766	780	893	1143[a]							$[Na]^+$, Aq. pH 6.0 [3]
8	$[V_9MoO_{28}]^{5-}$	27	436	786(C,C') 822(C")	801	895(E,E')	1153(F,F') 1169(F"')	1190	80	342		604	880	$[Na]^+$, Aq., pH *ca* 5-7[b] [2]
9*		27.6	438.7	786(C,C') 825(C")	806	896.8 930.1(E')	1143(F,F') 1180(F")	1170.8 1191(G')	80.2	337.2		604.4	881.4	$[Na]^+$, Aq., pH *ca* 6-7[b] [4]
10	$[HV_9MoO_{28}]^{4-}$	41.4	410.1	720 835.7	846.3 835.7	917.9 936	1187 1200	1200 1206.7	74.7	343.6		614.2	896.1	$[Na]^+$, Aq., pH *ca* 2[b] [4]
11*	*cis*-$[V_8Mo_2O_{28}]^{4-}$	77.2	446.7	726	832	909.2	1165	1207			279.4	622	922.2	$[Na]^+$, Aq., pH *ca* 1.5[b] [4]
12*	*trans*-$[V_8Mo_2O_{28}]^{4-}$	47.2		845	832	935	1198	1220			355.1	622	916	$[Na]^+$, Aq., pH *ca* 1.5[b] [4]

[a] Only one η-O signal was observed. [b] pH not explicitly indicated.

Table S6: Computed non-regressed ^{17}O NMR shifts of polyoxovanadates at PBE0/def2-tzvp//PBE0/cc-pvtz(H-Ar), lanl2dz(K-).

Entry	Anion	A μ_6-O	B μ_3-O	C μ_2-O	D μ_2-O	E μ_2-O	F η-O (V)	G η-O (V)	H OV_5M	I OV_2M	J OM_3	K VOM	L OM
1	$[V_2O_7]^{4-}$			405.7491			749.4465						
2	$[V_4O_{12}]^{4-}$			537.6781			986.4810						
3	$[V_{10}O_{28}]^{6-}$	72.9847	488.7242	822.8857	826.8696	923.8887	1168.6345	1165.2453					
4	$[V_9MoO_{28}]^{5-}$	121.0328	521.3673	845.4758, 845.2809(C,C') 868.0003(C")	843.9845	966.0855 932.6064(E')	1209.914, 1224.859(F,F') 1203.304(F")	1199.772 1219.654(G')	59.5768	425.9279		681.4618	929.3352
5	*cis*-$[V_8Mo_2O_{28}]^{4-}$	78.7002	526.2462	881.2569	881.9060	968.3087	1259.2853	1262.0740			357.5316	699.1630	970.5933
6	*trans*-$[V_8Mo_2O_{28}]^{4-}$	77.2633		886.7252	882.3726	969.5609	1260.1363	1260.6463			436.2515	695.8877	965.6687

Table S7: Experimentally determined ^{17}O NMR shifts of polyoxoniobates. The lettering indicates different oxygen sites, the type of which are specified in parentheses. See original publication and figures S10-S11 for assignment. Data used in regression is indicated with *.

Entry	Anion	A (μ_6-O)	B (μ_3-O)	C (μ_2-O)	D (μ_2-O)	E (μ_2-O)	G (η-O)	F (η-O)	Cation, Solvent [Ref.]
1	$[Nb_6O_{19}]^{8-}$	29		392		607			$[K]^+$, Aq., pH 14 [5]
2		20		386		594			Aq.,[a] pH 13 [6]
3*		11.8		396.8		580.3			$[K]^+$, Aq., pH 14.4 (see tables S16-S18) [7]
5		37		382		612			$[K]^+$, Aq., pH 11, $[OH]^-/[Nb_6O_{19}]^{8-}$=3 [8]
6		36		383		612			$[K]^+$, Aq., pH 11, $[OH]^-/[Nb_6O_{19}]^{8-}$=4 [8]
7		29		393		612			$[K]^+$, Aq., pH 13, $[OH]^-/[Nb_6O_{19}]^{8-}$=10 [8]
8		38		378		635			TMA, Aq., pH 11, $[OH]^-/[Nb_6O_{19}]^{8-}$=3 [8]
9		38		380		631			TMA, Aq., pH 11, $[OH]^-/[Nb_6O_{19}]^{8-}$=4 [8]
10		32		391		612			TMA, Aq., pH 13, $[OH]^-/[Nb_6O_{19}]^{8-}$=10 [8]
11	$[Nb_{10}O_{28}]^{6-}$	66.425	307.939	467.055	472.738	553.717	703.598	722.067	TMA, Aq. pH 5.5 [9]
12		66.033	308.218	466.623	472.959	553.922	703.879	722.184	TMA, Aq. pH 6.1 [9]
13		66.017	307.497	466.606	472.943	553.201	703.862	721.463	TMA, Aq. pH 6.6 [9]
14		66.017	307.497	466.606	472.943	553.201	703.862	721.463	TMA, Aq. pH 7.12 [9]
15		66.262	307.741	466.850	473.186	554.148	704.105	721.705	TMA, Aq. pH 7.51 [9]
16		66.377	307.857	466.967	473.303	553.562	703.519	721.823	TMA, Aq. pH 8.1 [9]
17		66.017	308.201	466.606	472.943	553.201	703.862	722.167	TMA, Aq. pH 8.5 [9]
18		66.377	307.857	466.967	473.303	553.562	703.519	721.823	TMA, Aq. pH 9.1 [9]
19*		66.050	308.234	466.640	472.976	553.939	703.896	722.201	TMA, Aq. pH 9.6 [9]
20	$[TiNb_9O_{28}]^{7-}$	74.920	300.399	452.760	462.845	546.770	673.557	691.206	TMA, Aq. pH 6.54[9]
			341.101 (B')	458.523 (C')		592.514 (E')	670.676 (G')		
21		74.559	300.399	452.760	462.845	546.409	673.196	690.125	TMA, Aq. pH 7.05[9]
			340.740 (B')	458.883 (C')		592.874 (E')	670.315 (G')		
22		74.920	299.679	452.760	461.764	547.130	676.798	692.287	TMA, Aq. pH 7.92[9]
			338.219 (B')	458.163 (C')		590.713 (E')	673.557 (G')		
23		74.920	300.399	453.120	462.845	546.770	673.917	690.486	TMA, Aq. pH 8.95[9]
			341.101 (B')	458.883 (C')		593.594 (E')	671.036 (G')		
24		74.920	300.399	453.120	462.845	546.770	673.557	690.486	TMA, Aq. pH 9.96[9]
			341.101 (B')	458.883 (C')		594.594 (E')	670.675 (G')		
25		74.560	300.039	453.121	462.846	546.410	672.837	690.487	TMA, Aq. pH 10.98[9]
			340.741 (B')	458.884 (C')		594.235 (E')	670.316 (G')		
26		74.559	300.039	452.760	462.485	546.409	673.196	690.125	TMA, Aq. pH 11.63[9]
			340.740 (B')	458.523 (C')		593.234 (E')	670.315 (G')		
27		74.560	300.039	453.120	462.845	546.410	672.837	690.486	TMA, Aq. pH 12.47[9]
			340.741 (B')	458.883 (C')		593.235 (E')	670.315 (G')		
28		74.199	300.039	452.760	462.485	546.049	672.116	689.405	TMA, Aq. pH 13.25[9]
			340.740 (B')	458.523 (C')		592.874 (E')	669.955 (G')		
29	$[Ti_2Nb_8O_{28}]^{8-}$	101.934	331.735		451.678	555.773	666.712	680.399	TMA, Aq. pH 6.61 [9]
30		99.413	331.736		451.679	558.296	662.751	677.519	TMA, Aq. pH 7.15 [9]
31		97.972	332.096		451.319	561.177	661.310	676.438	TMA, Aq. pH 7.49 [9]
32*		89.327	328.854	431.508	449.158	575.225	652.666	669.234	TMA, Aq. pH 8.03 [9]
33		88.247	329.214	434.750	449.518	576.666	650.505	667.794	TMA, Aq. pH 8.52 [9]
34		87.887	329.575	435.471	449.518	577.746	649.424	666.713	TMA, Aq. pH 8.95 [9]
35		86.806	331.015	434.750	449.878	579.547	645.462	664.192	TMA, Aq. pH 9.43 [9]
36		85.725	330.655	436.191	449.158	580.267	644.381	663.111	TMA, Aq. pH 10.01 [9]
37		85.725	331.015	436.911	449.517	580.626	644.380	663.110	TMA, Aq. pH 10.45 [9]
38*		85.725	331.015	436.911	449.518	580.988	644.381	663.111	TMA, Aq. pH 10.79 [9]

[a] Counterion not indicated.

Table S8: Computed non-regressed ^{17}O NMR shifts of polyoxoniobates at PBE0/def2-tzvp//PBE0/cc-pvtz(H-Ar), lanl2dz(K-).

Entry	Anion	A (μ_6-O)	B (μ_3-O)	C (μ_2-O)	D (μ_2-O)	E (μ_2-O)	F (η-O)	G (η-O)
1	$[Nb_6O_{19}]^{8-}$	70.7060		464.7897		641.7471		
2	$[Nb_{10}O_{28}]^{6-}$	121.6874	364.8398	536.6640	525.7640	611.8384	794.7706	766.5670
3	$[TiNb_9O_{28}]^{7-}$	138.1742	352.9244 (B)	528.4199 (C')	517.6431	608.2108 (E)	767.5604	742.7352 (G')
			398.3550 (B')	529.1051 (C)		659.8050 (E')		750.1919 (G)
4	$[Ti_2Nb_8O_{28}]^{8-}$	148.9896	385.9111	514.4733	500.1411	648.0585	734.7198	714.2441

Table S9: Experimentally determined ^{17}O NMR shifts of polyoxotantalates. The lettering indicates different oxygen sites, the type of which are specified in parentheses. See original publication and figures S10-S11 for assignment. Data used in regression is indicated with *.

	Anion	A (μ_6-O)	B (μ_3-O)	C (μ_2-O)	D (μ_2-O)	E (μ_2-O)	F (η-O)	G (η-O)	Cation, Solvent [Ref.]
1*	$[Ta_6O_{19}]^{8-}$	-39	328				478		K^+, Aq., pH 14 [5]
2		-41	329				476		Aq.,[a] pH 13 [6]
3*	$[Ta_{10}O_{28}]^{6-}$	26	249	398	385	461	591	571	TBA, Aq./ACN[b] [8]

[a] Counterion not indicated. [b] pH not indicated.

Table S10: Computed non-regressed ^{17}O NMR shifts of polyoxotantalates at PBE0/def2-tzvp//PBE0/cc-pvtz(H-Ar), lanl2dz(K-).

	Anion	A (μ_6-O)	B (μ_3-O)	C (μ_2-O)	D (μ_2-O)	E (μ_2-O)	F (η-O)	G (η-O)
1	$[Ta_6O_{19}]^{8-}$	71.8385	371.5893				525.3828	
2	$[Ta_{10}O_{28}]^{6-}$	121.5488	305.6237	433.3515	417.6975	498.6297	652.0944	624.0150

Table S11: Experimentally determined ^{17}O NMR shifts of polyoxomolybdates. The lettering indicates different oxygen sites, the type of which are specified in parentheses. See original publication and figures S10-S11 for assignment. Data used in regression is indicated with *.

	Anion	A μ_6-O	B OMo_3	C OMo_2	D OMo_2	E OMo_2	F (η-O (Mo))	G (η-O (Mo))	H MOMo	I OM_2	J (η-O (M))	Cation, Solvent [Ref.]
1*	$[Mo_6O_{19}]^{2-}$	-32		559			927					TBA, DMF [5, 10]
2				563			933					TBA, ACN [5]
3*	$[VMo_5O_{19}]^{3-}$	-22		541	531		885		665		1200	TBA, ACN [5]
4*	$[V_2Mo_4O_{19}]^{4-}$			489	498		862		604		1165	$[Na]^+$, Aq. [2]
5*	$[TeMo_6O_{24}]^{6-}$		180	383			807					$[Na]^+$, Aq. pH 5.8 [5]
6*	$[H_6AlMo_6O_{24}]^{3-}$			378			833					$[Na]^+$, Aq. pH 4.1 [5]
		μ_4-O										
7	$[Mo_7O_{24}]^{6-}$	123	338	400	758		821					$[Na]^+$, Aq. pH 5.5 [11]
8		123	335	395	757		814					$[Na]^+$, Aq. pH 5.5 [5]
9		123	340	398	759		824					$[NH_4]^+$, Aq. pH 5.4 [5]
10*		122	340	397	750		817(F)					$[NH_4]^+$, Aq.,[a][12]
			354		757		824(F',F")					
11*	α–$[Mo_8O_{26}]^{4-}$		495	396	775		866					TBA, ACN, [5, 10]
12*	β–$[Mo_8O_{26}]^{4-}$	56	296	425	743		866	900(F,F',F",F"')				TBA, ACN [5, 10]
13*	$[PMo_{12}O_{40}]^{3-}$	78		583	550		936					TBA, ACN [5]
14*	$[SiMo_{12}O_{40}]^{4-}$	41		580	555		928					TBA, ACN [5]
15*	$[GaMo_{12}O_{40}]^{5-}$			575	568		923					$[H]^+$, Aq. [13]

[a] pH not given.

Table S12: Computed non-regressed ^{17}O NMR shifts of polyoxomolybdates at PBE0/def2-tzvp//PBE0/cc-pvtz(H-Ar), lanl2dz(K-).

	Anion	A μ_6-O	B OMo_3	C OMo_2	D OMo_2	E OMo_2	F (η-O (Mo))	G (η-O (Mo))	H MOMo	I OM_2	J (η-O (M))
1	$[Mo_6O_{19}]^{2-}$	24.1773		634.4282			1006.6900				
2	$[VMo_5O_{19}]^{3-}$	-2.1462		587.1757	580.6522		955.1359		703.6874		1278.9114
3	$[V_2Mo_4O_{19}]^{4-}$			547.4077	653.1606		894.5740		692.2472		1185.3398
4	$[TeMo_6O_{24}]^{6-}$		247.2371	472.8190			862.6313				
5	$[H_6AlMo_6O_{24}]^{3-}$			480.4051			918.2591				
		μ_4-O									
6	$[Mo_7O_{24}]^{6-}$	202.1697	436.1738 452.7282	497.0060	781.1074 785.1972		873.1187(F) 882.3631(F',F")	833.9954			
7	α–$[Mo_8O_{26}]^{4-}$		557.6329	483.9945	850.9894		928.0600				
9	$[PMo_{12}O_{40}]^{3-}$	134.9841		653.2265	622.8281		1011.6802				
10	$[SiMo_{12}O_{40}]^{4-}$	96.4548		651.1499	625.8577		1007.1545				
11	$[GaMo_{12}O_{40}]^{5-}$			662.4293	634.1072		995.0366				
		μ_5-O									
8	β–$[Mo_8O_{26}]^{4-}$	124.3076	410.3020	499.3071	802.7165		932.7817(F) 917.3511(F') 926.5983(F") 955.9130(F"')	962.4964			

Table S13: Experimentally determined ^{17}O NMR shifts of polyoxotungstates. The lettering indicates different oxygen sites, the type of which are specified in parentheses. See original publication and figures S10-S11 for assignment. Data used in regression is indicated with *.

	Anion	A μ_6-O	B OW_3	C OW_2	D OW_2	E OW_2	F (η-O (W))	G (η-O (W))	W-O-M	OM_2	(η-O (M))	Cation, Solvent [Ref.]
1*	$[W_6O_{19}]^{2-}$	-81		413			772					TBA, DMF [14, 5]
2*	$[NbW_5O_{19}]^{3-}$	-67		392	394		730	732	456		799	TBA, ACN [15]
3*	$[TaW_5O_{19}]^{3-}$	-73		93	394		731	733	420		666	TBA, ACN [15]
4*	$[VW_5O_{19}]^{3-}$	-75		395	389		731		562		1217	TBA, ACN [14, 5]
5*	$[TiW_5(OMe)O_{18}]^{3-}$	-58		380	390		713	721	525			TBA, ACN [16]
6*	$[SnW_5(OMe)O_{18}]^{3-}$	17		363	383		684	720	395			TBA, ACN [17]
7*	$[Nb_2W_4O_{19}]^{4-}$			374			691		435(H,H')	493	753	TBA, ACN [15]
8*	$[V_2W_4O_{19}]^{4-}$	-65		371	384		687		530(H,H')	848	1162	TBA, ACN [14]
9*	$[W_{10}O_{32}]^{4-}$	-6		430	416		762					TBA, ACN [5]
		-1.6		434	421	423	765	732				TBA, ACN [18]
		μ_4-O										
10*	$[W_7O_{24}]^{6-}$	71	254 295	314	590	595	648(F,F',F")	624				$[Na]^+$, Aq.[a] [12]
11*	$[BW_{12}O_{40}]^{5-}$	49		410			740					$[Na]^+$, Aq., pH 6.5-7.0[a] [19]
12*	$[PW_{12}O_{40}]^{3-}$			431	405		769					TBA, Aq.[a] [5]
		68		429	410		770					TBA, ACN [20]
13*	$[SiW_{12}O_{40}]^{4-}$	27		427	405		761					TBA, ACN [5, 20]
14*	$[GaW_{12}O_{40}]^{5-}$			417	410		756					$[H]^+$, Aq.[a] [21, 20]

[a] pH not given or not explicitly given.

Table S14: Computed non-regressed ^{17}O NMR shifts of polyoxotungstates at PBE0/def2-tzvp//PBE0/cc-pvtz(H-Ar), lanl2dz(K-).

	Anion	A μ_6-O	B OW_3	C OW_2	D OW_2	E OW_2	F (η-O (W))	G (η-O (W))	H W-O-M	I OM_2	J (η-O (M))
1	$[W_6O_{19}]^{2-}$	27.1091		471.6662			807.2543				
2	$[NbW_5O_{19}]^{3-}$	26.6769		447.3100			768.7669		507.8898		843.8781
3	$[TaW_5O_{19}]^{3-}$	33.2494		448.4662			768.0084		469.9926		692.2944
4	$[VW_5O_{19}]^{3-}$	19.1239		448.8332			769.9133		599.8506		1264.4884
5	$[TiW_5(OMe)O_{18}]^{3-}$	36.7791		437.2122	444.0949		748.4535	755.1191	570.8406		
6	$[SnW_5(OMe)O_{18}]^{3-}$	97.7043		414.1766	438.8812		713.5677	750.2890	451.0481		
7	$[Nb_2W_4O_{19}]^{4-}$	40.6921		429.1183			732.5865		485.6050 483.5458	547.9321	796.4729
8	$[V_2W_4O_{19}]^{4-}$	22.8015		428.8062			846.7756		563.4016 556.4016(H')	762.6024	1199.6009
9	$[W_{10}O_{32}]^{4-}$	75.7722 μ_4-O		458.9297	473.5959	484.6224	770.3677	803.9238			
10	$[W_7O_{24}]^{6-}$	153.9535	327.3486 357.6217	381.8083	637.3061	649.9097	699.0286 692.4312(F',F")	664.5313			
11	$[BW_{12}O_{40}]^{5-}$	113.2042		450.9616	471.4723		785.5085				
12	$[PW_{12}O_{40}]^{3-}$	135.8173		455.1303	487.9224		805.3313				
13	$[SiW_{12}O_{40}]^{4-}$	97.4293		453.5796	486.0730		803.9524				
14	$[GaW_{12}O_{40}]^{5-}$			455.6311	493.4255		801.1723				

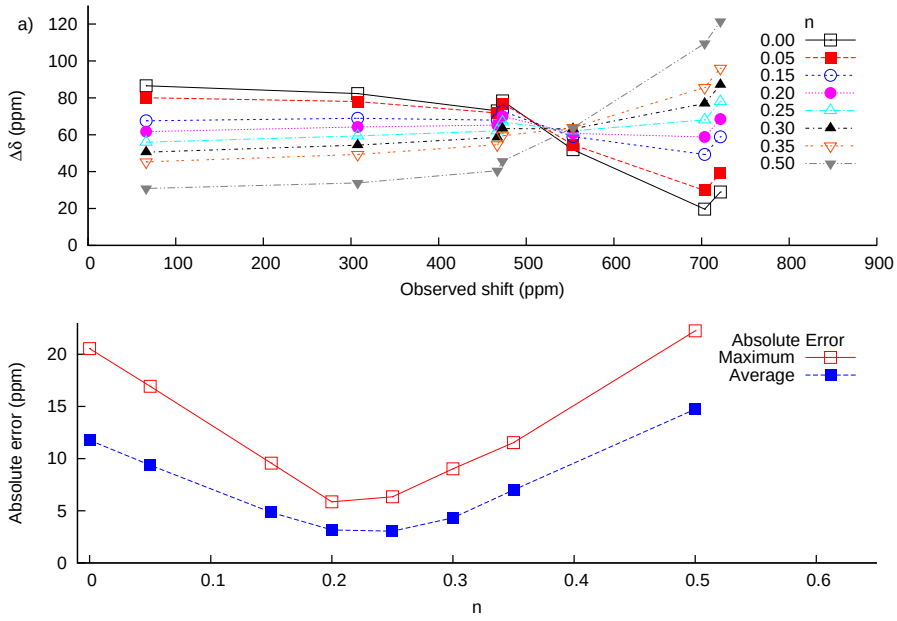

Figure S6: Effect on the calculated non-regressed ^{17}O NMR chemical shift of $[Nb_{10}O_{28}]^{6-}$ of varying the HF-exchange-to-PW91-exchange ratio using n in the exchange correlation functional XC=n·HF$_{ex}$+(n-1)·PW91$_{ex}$)+PW91$_{corr}$, and b) effect on the maximum and average error in the calculated linearly regressed ^{17}O NMR chemical shift. All shift calculations were done using def2-tzvp and with implicit solvation using PCM (water), and using a structure optimised at PBE0/cc-pvtz(H-Ar), lanl2dz(K-).

```
K=[10^(-9.35) 10^(-9.92) 10^(-13.63)];
h=logspace(-9,-14,100);
Ctot=1.0;
species=speciation(K,h,Ctot);
plot(-log10(h),species(:,:))
```

Listing S1: control.m

```
function curve=speciation(k,h,ctot)
  k=[1 k];

  for n=1:size(k,2)
    knew(n,1)=prod(k(1,1:n),2);
    hnew(n,:)=h.^(n-1)';
  end
  vector=(knew'./hnew');
  c=vector(:,2);
  c=ctot./sum(vector,2);
  curve=[c.*vector];
end
```

Listing S2: speciation.m

Table S15: Computed non-regressed ^{17}O NMR shifts in ppm of protonated and unprotonated structures of $[Nb_6O_{19}]^{8-}$ at PBE0/def2-tzvp//PBE0/cc-pvtz(H-Ar), lanl2dz(K-). The different isomers are listed in the same order as in figure S8. The lowest energy isomers at pbe0/def2-tzvp are marked with bold; $\Delta\epsilon$ is given relative to the lowest energy isomer for each protonation state.

Entry	Number of protons	δ μ_6-O	δ μ_2-O	δ η=O	ϵ (a.u.)	$\Delta\epsilon$ (kcal)
1	0	**71**	**465**	**642**	-1772.79383817	0
2	1	**89**	**452**	**679**	-1773.32865682	0
3	2	100	438	715	-1773.84487818	0.4391
4		99	437	714	-1773.84142771	2.6043
5		105	442	718	-1773.83768080	4.9555
6		105	442	720	-1773.83737179	5.1494
7		**98**	**439**	**722**	-1773.84557801	0
8		97	438	722	-1773.84547981	0.0616
9		105	439	721	-1773.8406571	3.0879
10		107	439	720	-1773.84094689	2.9060
11	3	109	421	757	-1774.3391972	5.3238
12		111	423	759	-1774.3388020	5.5718
13		**99**	**415**	**757**	-1774.3476813	0
14		111	426	757	-1774.33818085	5.9616
15		103	422	758	-1774.34387887	2.3860
16		106	422	749	-1774.34226680	3.3976
17		120	430	762	-1774.32708771	12.923
18		121	430	762	-1774.32677228	13.120
19		112	422	756	-1774.34242317	3.2995
20		120	430	762	-1774.32713339	12.894
21		112	422	755	-1774.34196575	3.5865
22		120	430	762	-1774.32712675	12.898
23		111	425	755	-1774.33816727	5.9701
24		109	423	754	-1774.33525822	7.7955
25		110	430	776	-1774.32831278	12.154
26		110	422	758	-1774.33525822	7.7955
27		112	422	755	-1774.34200367	3.5627
28		122	441	780	-1774.31576440	20.028
29		120	430	762	-1774.32712033	12.902
30		112	422	756	-1774.34242370	3.2992
31		120	430	762	-1774.32708035	12.927
32		121	430	762	-1774.32677621	13.118

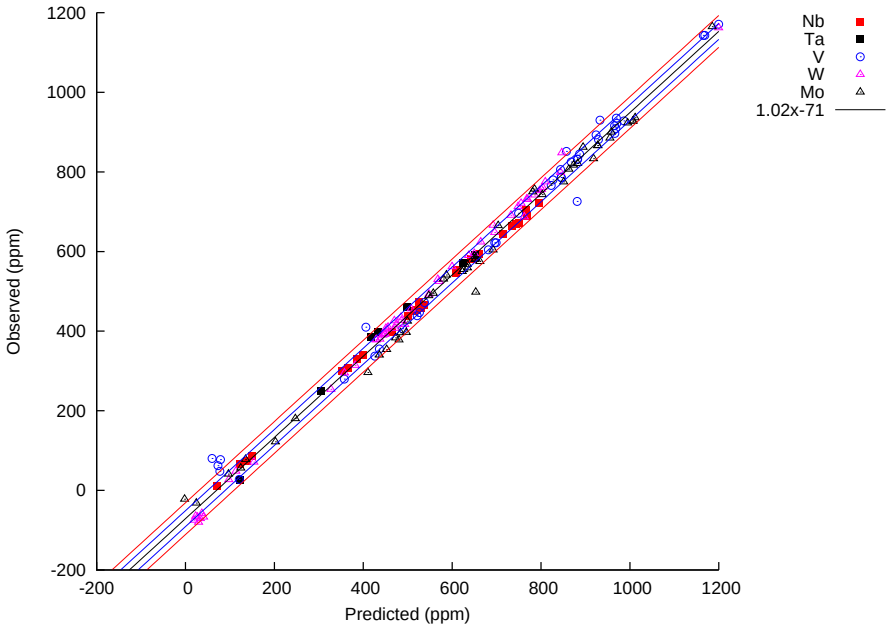

Figure S7: Predicted vs observed ^{17}O NMR chemical shifts for all the compounds in the test set. The coefficient of determination is 0.993.

Table S16: Extracted chemical shifts for the η-oxygen site in the hexaniobate ion as a function of pH. The data was extracted from figure 4 in Black *et al.*, *J. Am. Chem. Soc.*, **2006**, *128*, 14712-14720.

Temperature (K)	pH	Shift (ppm)
277	10.11	626.96
	10.25	625.58
	10.36	624.61
	11.06	615.64
	11.35	610.52
	12.39	602.79
	12.96	601.13
	13.33	598.51
	13.39	598.92
	14.30	586.08
298	11.11	612.87
	11.22	610.52
	12.25	604.17
	12.64	602.10
	13.11	600.03
	13.52	594.78
	13.67	592.43
	13.98	587.04
	14.43	580.28
303	12.91	599.75

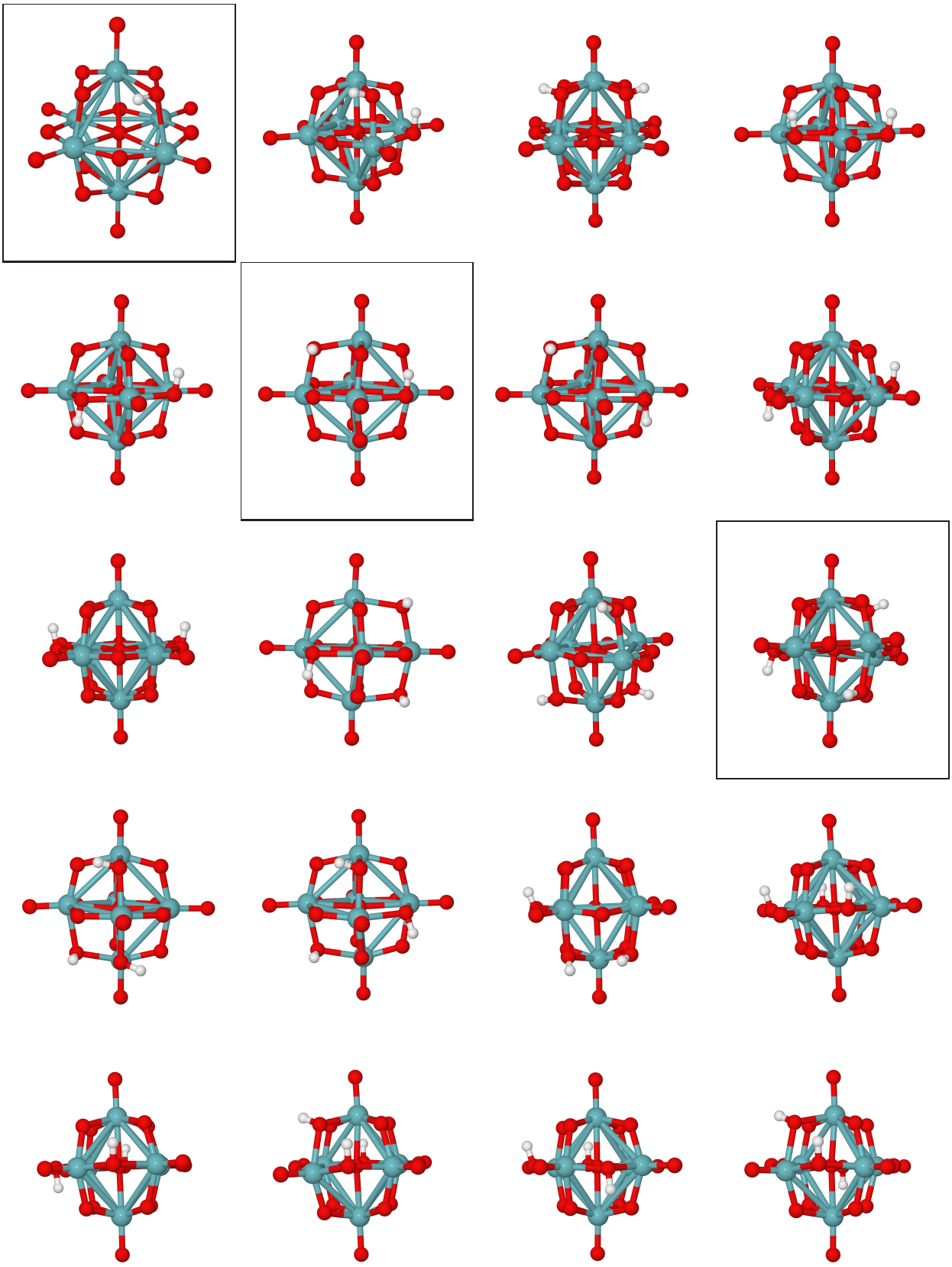

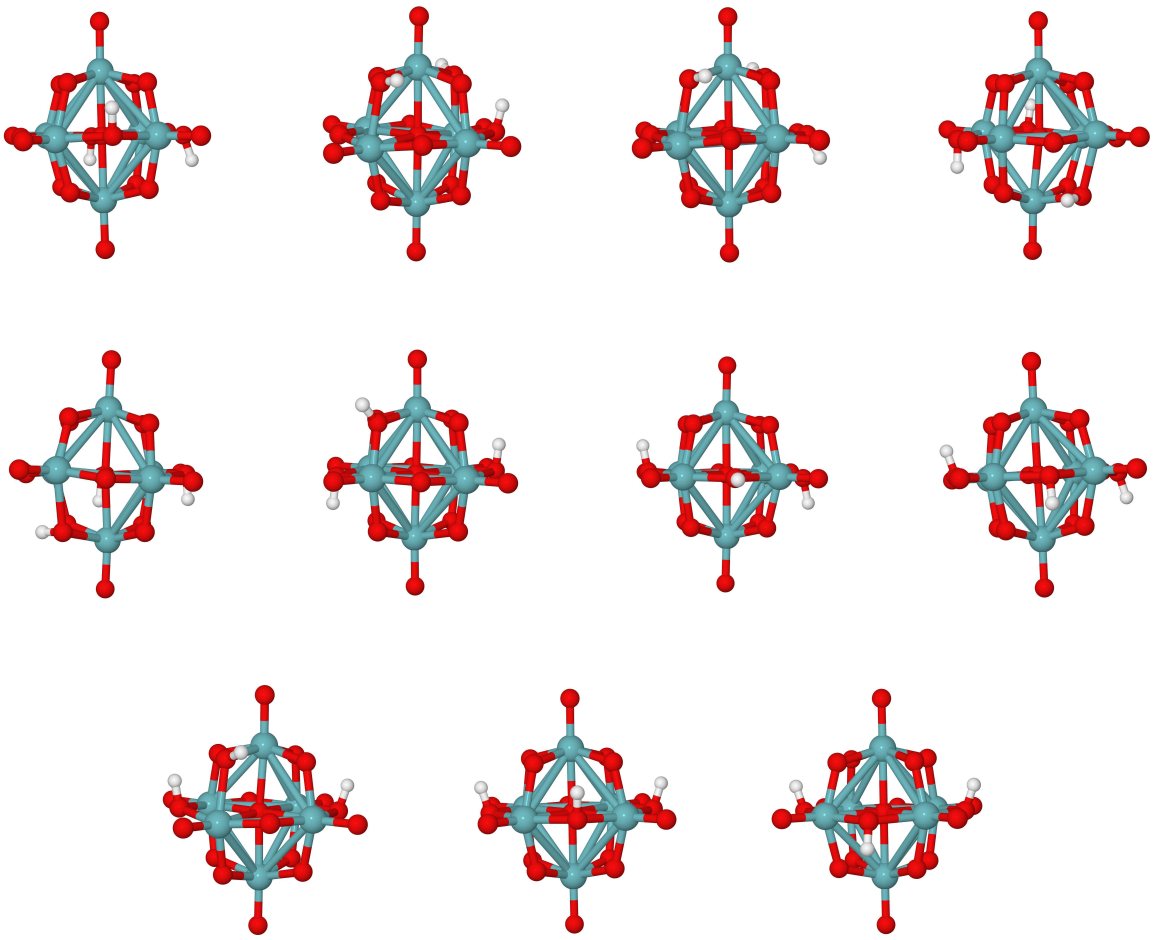

Figure S8: The lowest energy isomers for each protonation state are framed. From left to right, top row (energy in parenthesis): $[HNb_6O_{19}]^{7-}$ (-1773.32865682 a.u.), $[H_2Nb_6O_{19}]^{6-}$ (-1773.84487818 a.u.), $[H_2Nb_6O_{19}]^{6-}$ (-1773.84142771 a.u.) and $[H_2Nb_6O_{19}]^{6-}$ (-1773.8376808 a.u.). Second row: $[H_2Nb_6O_{19}]^{6-}$ (-1773.83737179 a.u.), $[H_2Nb_6O_{19}]^{6-}$ (-1773.84557801 a.u.), $[H_2Nb_6O_{19}]^{6-}$ (-1773.84547981 a.u.) and $[H_2Nb_6O_{19}]^{6-}$ (-1773.8406571 a.u.). Third row: $[H_2Nb_6O_{19}]^{6-}$ (-1773.84094689 a.u.), $[H_3Nb_6O_{19}]^{6-}$ (-1774.3391972 a.u.), $[H_3Nb_6O_{19}]^{6-}$ (-1774.338802 a.u.) and $[H_3Nb_6O_{19}]^{6-}$ (-1774.3476813 a.u.). Fourth row: $[H_3Nb_6O_{19}]^{6-}$ (-1774.33818085 a.u.), $[H_3Nb_6O_{19}]^{6-}$ (-1774.34387887 a.u.), $[H_3Nb_6O_{19}]^{6-}$ (-1774.34226680 a.u.) and $[H_3Nb_6O_{19}]^{6-}$ (-1774.32708771 a.u.). Fifth row: $[H_3Nb_6O_{19}]^{6-}$ (-1774.32677228 a.u.), $[H_3Nb_6O_{19}]^{6-}$ (-1774.34242317 a.u.), $[H_3Nb_6O_{19}]^{6-}$ (-1774.32713339 a.u.) and $[H_3Nb_6O_{19}]^{6-}$ (-1774.34196575 a.u.). Sixth row: $[H_3Nb_6O_{19}]^{6-}$ (-1774.32712675 a.u.), $[H_3Nb_6O_{19}]^{6-}$ (-1774.33816727 a.u.), $[H_3Nb_6O_{19}]^{6-}$ (-1774.33525822 a.u.) and $[H_3Nb_6O_{19}]^{6-}$ (-1774.32831278 a.u.). Seventh row: $[H_3Nb_6O_{19}]^{6-}$ (-1774.33525822 a.u.), $[H_3Nb_6O_{19}]^{6-}$ (-1774.34200367 a.u.), $[H_3Nb_6O_{19}]^{6-}$ (-1774.31576440 a.u.) and $[H_3Nb_6O_{19}]^{6-}$ (-1774.32712033 a.u.). Eighth row: $[H_3Nb_6O_{19}]^{6-}$ (-1774.34242370 a.u.), $[H_3Nb_6O_{19}]^{6-}$ (-1774.32708035 a.u.) and $[H_3Nb_6O_{19}]^{6-}$ (-1774.32677621 a.u.)

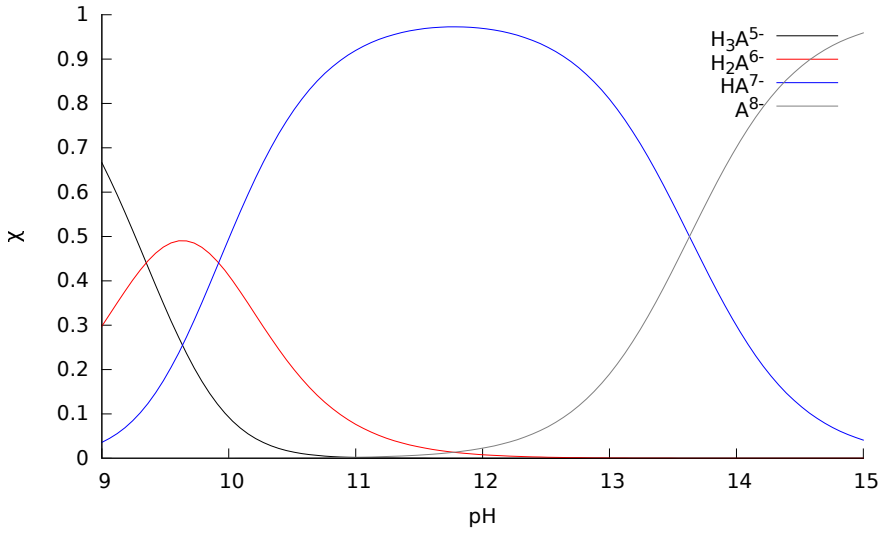

Figure S9: Speciation of the hexaniobate Lindqvist ion as a function of pH simulated using the Octave code in listings S1 and S2.

Table S17: Extracted chemical shifts for the μ_2-oxygen site in the hexaniobate ion as a function of pH. The data was extracted from figure 4 in Black *et al.*, *J. Am. Chem. Soc.*, **2006**, *128*, 14712-14720.

Temperature (K)	pH	Shift (ppm)
277	10.14	376.85
	10.24	377.40
	10.37	378.49
	11.06	380.55
	11.36	383.70
	12.40	386.99
	12.97	387.95
	13.33	389.04
	13.40	390.00
	14.30	395.62
298	11.11	382.19
	11.23	383.15
	12.25	387.67
	12.65	387.81
	13.13	389.32
	13.54	390.82
	13.69	392.05
	13.99	394.25
	14.46	396.85
303	12.93	388.63

Table S18: Extracted chemical shifts for the μ_6-oxygen site in the hexaniobate ion as a function of pH. The data was extracted from figure 4 in Black *et al.*, *J. Am. Chem. Soc.*, **2006**, *128*, 14712-14720.

Temperature (K)	pH	Shift (ppm)
277.00	10.13	31.10
	10.25	30.41
	10.36	30.27
	11.06	27.26
	11.36	25.62
	12.40	22.74
	12.96	21.92
	13.33	21.10
	13.39	21.51
	14.30	15.07
298.00	11.11	26.44
	11.23	25.75
	12.25	24.25
	12.64	24.25
	13.11	22.05
	13.53	19.59
	13.68	18.08
	13.99	15.48
	14.44	11.78
303.00	12.92	21.78

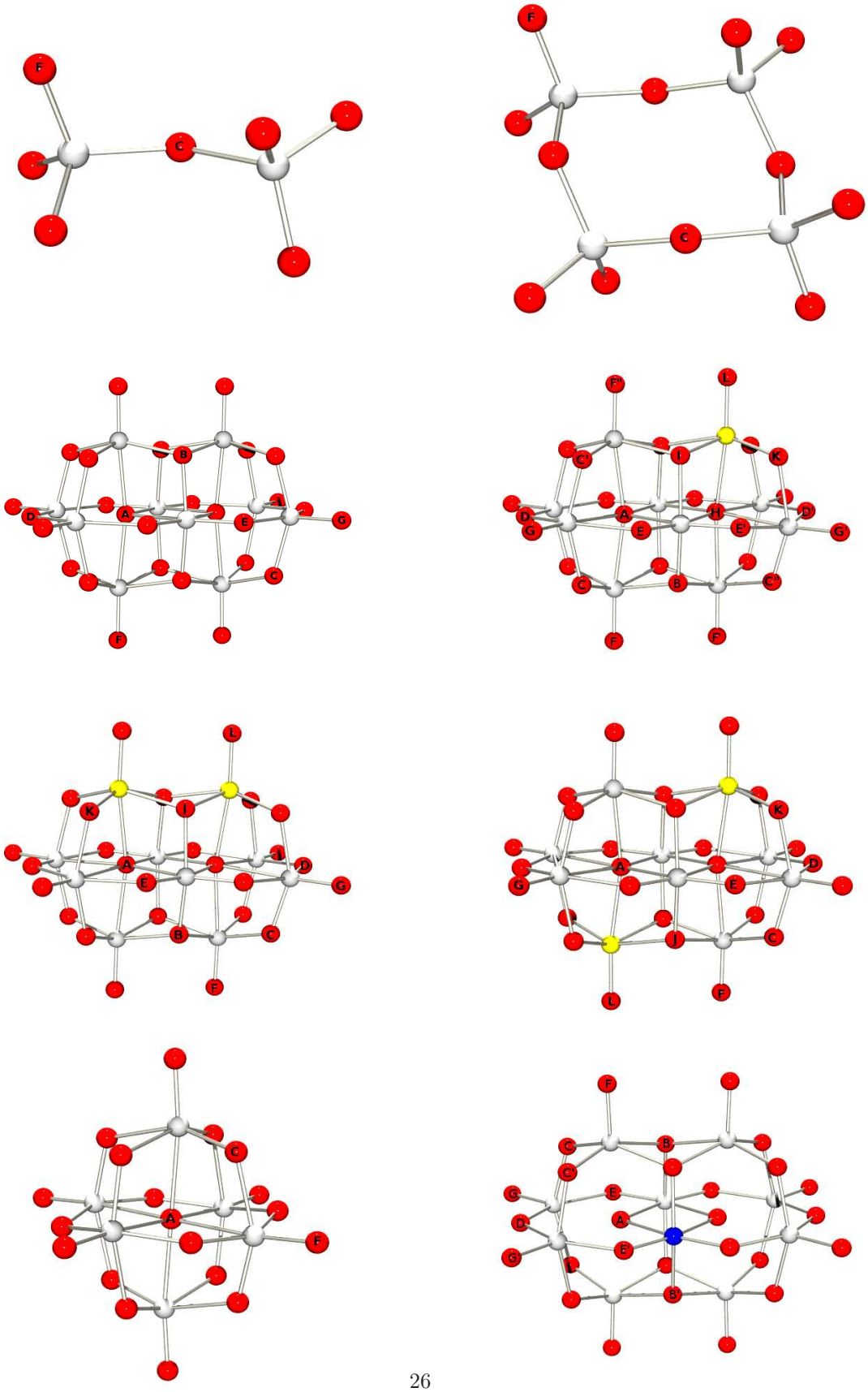

Figure S10: Key I to oxygen types referred to in tables S5-S14. Row 1, left: $[V_2O_7]^{4-}$. Right: $[V_4O_{12}]^{4-}$. Row 2, left: $[M_{10}O_{28}]^{x-}$. Right: $[V_9MoO_{28}]^{5-}$. Row 3, left: cis–$[V_8Mo_2O_{28}]^{4-}$. Right: trans–$[V_8Mo_2O_{28}]^{4-}$. Row 4, left: $[M_6O_{19}]^{x-}$. Right: $[TiNb_9O_{28}]^{7-}$.

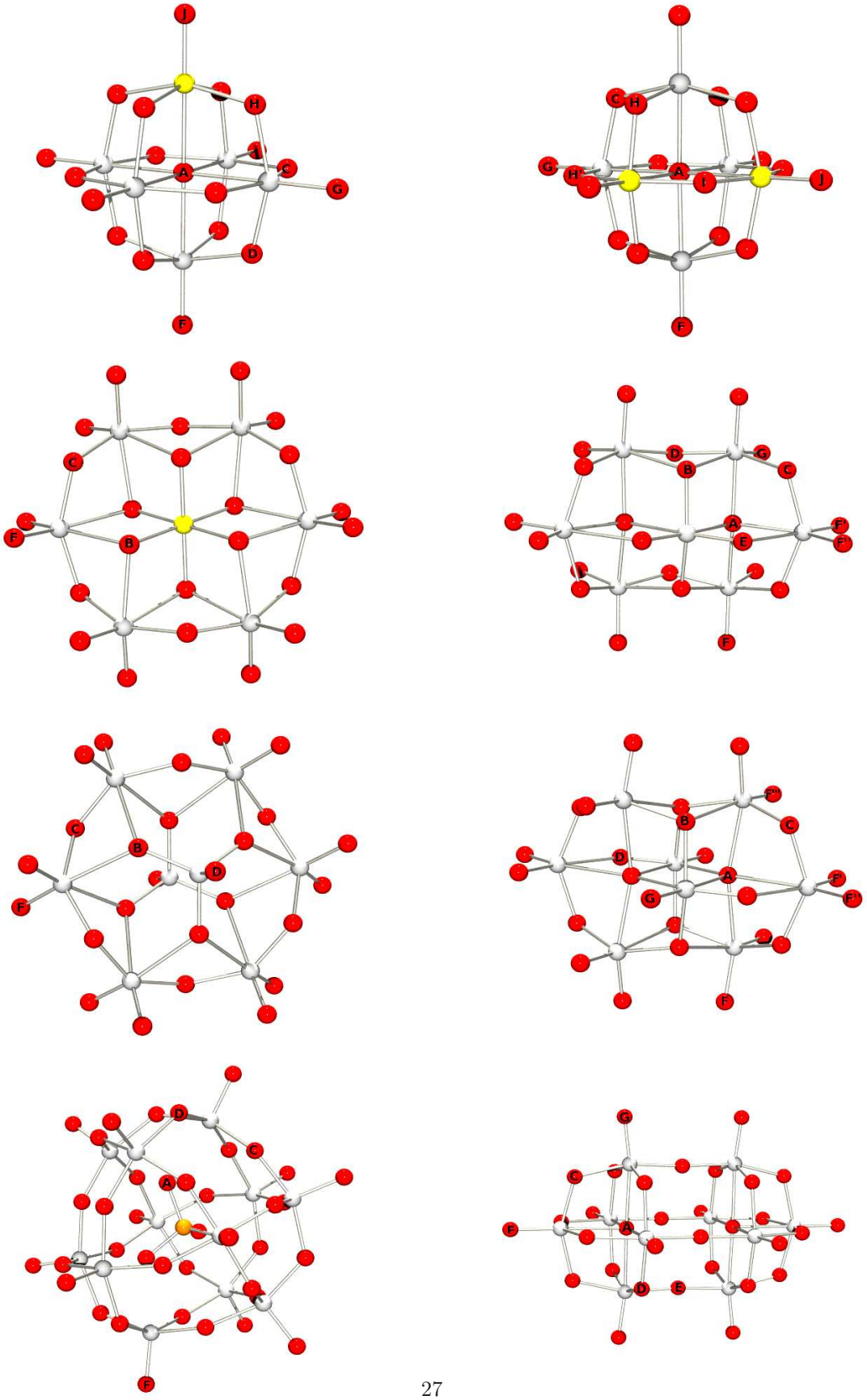

Figure S11: Key II to oxygen types referred to in tables S5-S14. Row 1, left: $[M_5O_{19}]^{x-}$ and $[M(OMe)M_5O_{18}]^{x-}$. Right: $[M_2M_4O_{19}]^{x-}$. Row 2, left: $H_n[MMo_6O_{24}]^{x-}$. Right: $[M_7O_{24}]^{6-}$. Row 3, left: α–$[Mo_8O_{26}]^{4-}$. Right: β–$[Mo_8O_{26}]^{4-}$. Row 4, left: $[MM_{12}OO_{40}]^{x-}$. Right: $[W_{10}O_{32}]^{4-}$.

References

[1] E. Heath, O. W. Howarth, *J. Chem. Soc., Dalton Trans.* **1981**, *5*, 1105–1110.

[2] R. I. Maksimovskaya, N. N. Chumachenko, *Polyhedron* **1987**, *6*, 1813–1821.

[3] W. G. Klemperer, W. Shum, *J. Am. Chem. Soc.* **1977**, *99*, 3544–3545.

[4] O. W. Howarth, *J. Chem. Soc., Dalton Trans.* **1989**, *10*, 1915–1923.

[5] M. Filowitz, R. K. C. Ho, W. G. Klemperer, W. Shum, *Inorg. Chem.* **1979**, *18*, 93–103.

[6] A. D. English, J. P. Jesson, W. G. Klemperer, T. Mamouneas, L. Messerle, W. Shum, A. Tramontano, *J. Am. Chem. Soc.* **1975**, *97*, 4785–4786.

[7] J. R. Black, M. Nyman, W. H. Casey, *J. Am. Chem. Soc.* **2006**, *128*, 14712–14720.

[8] W. G. Klemperer, K. A. Marek, *Eur. J. Inorg. Chem.* **2013**, 1762–1771.

[9] E. M. Villa, Personal communication.

[10] W. G. Klemperer, *Angew. Chem. Int. Ed. Engl.* **1978**, *17*, 246–254.

[11] W. G. Filowitz, M. Klemperer, W. Messerle, L.and Shum, *J. Am. Chem. Soc.* **1976**, *98*, 2345–2346.

[12] R. I. Maksimovskaya, K. G. Burtseva, *Polyhedron* **1985**, *4*, 1559–1562.

[13] L. P. Tsiganok, A. B. Vishnikin, R. I. Maksimovskaya, *Polyhedron* **1989**, *8*, 2739–2742.

[14] W. G. Klemperer, W. Shum, *J. Am. Chem. Soc.* **1978**, 4891–4893.

[15] C. J. Besecker, W. G. Klemperer, D. J. Maltibie, D. A. Wright, *Inorg. Chem.* **1985**, *24*, 1027–1032.

[16] R. J. Errington, S. S. Petkar, P. S. Middleton, W. McFarlane, W. Clegg, R. A. Coxall, R. W. Harrington, *Dalton Trans.* **2007**, 5211–5222.

[17] B. Kandasamy, C. Wills, W. McFarlane, W. Clegg, R. W. Harrington, Rodríguez-Fortea, J. M. Poblet, P. G. Bruce, R. J. Errington, *Chem. Eur. J.* **2012**, *18*, 59–62.

[18] D. C. Duncan, C. L. Hill, *RSC Adv.* **2014**, *4*, 7094–7103.

[19] R. I. Maksimovskaya, G. M. Maksimov, *Inorg. Chem.* **2011**, *50*, 4725–4731.

[20] R. I. Maksimovskaya, M. A. Fedotov, *J. struc. Chem.* **2006**, *47*, 1559–1562.

[21] L. P. Kazansky, M. A. Fedotov, *Izv. Akad. Nuak SSSR, Ser. Khim.* **1988**, *9*, 2000–2003.